

Spatiotemporal Differences in CXCL12 Expression and Cyclic AMP Underlie the Unique Pattern of Optic Glioma Growth in Neurofibromatosis Type 1

Nicole M. Warrington,¹ B. Mark Woerner,¹ Girish C. Dagainakatte,² Biplab Dasgupta,² Arie Perry,³ David H. Gutmann,² and Joshua B. Rubin^{1,2,4}

Departments of ¹Pediatrics, ²Neurology, ³Pathology, and ⁴Anatomy and Neurobiology, Washington University School of Medicine, St. Louis, Missouri

Abstract

Astrocytoma (glioma) formation in neurofibromatosis type 1 (NF1) occurs preferentially along the optic pathway during the first decade of life. The molecular basis for this unique pattern of gliomagenesis is unknown. Previous studies in mouse *Nf1* optic glioma models suggest that this patterning results from cooperative effects of *Nf1* loss in glial cells and the action of factors derived from the surrounding *Nf1*+/- brain. Because CXCL12 is a stroma-derived growth factor for malignant brain tumors, we tested the hypothesis that CXCL12 functions in concert with *Nf1* loss to facilitate NF1-associated glioma growth. Whereas CXCL12 promoted cell death in wild-type astrocytes, it increased *Nf1*-/- astrocyte survival. This increase in *Nf1*-/- astrocyte survival in response to CXCL12 was due to sustained suppression of intracellular cyclic AMP (cAMP) levels. Moreover, the ability of CXCL12 to suppress cAMP and increase *Nf1*-/- astrocyte survival was a consequence of mitogen-activated protein/extracellular signal-regulated kinase kinase-dependent inhibition of CXCL12 receptor (CXCR4) desensitization. In support of an instructive role for CXCL12 in facilitating optic glioma growth, we also show that CXCL12 expression along the optic pathway is higher in infant children and young mice and is associated with low levels of cAMP. CXCL12 expression declines in multiple brain regions with increasing age, correlating with the age-dependent decline in glioma growth in children with NF1. Collectively, these studies provide a mechanism for the unique pattern of NF1-associated glioma growth. [Cancer Res 2007;67(18):8588–95]

Introduction

Neurofibromatosis type 1 (NF1) is an autosomal dominant tumor predisposition syndrome that affects ~1:3,000 people worldwide (1). Individuals with NF1 are susceptible to a variety of neoplasms but are especially prone to the development of benign and malignant tumors of the peripheral and central nervous systems (2). Approximately 15% of patients with NF1 develop low-grade astrocytomas that derive from a transformed glial fibrillary acidic protein (GFAP)-positive cell (astroglial cell) in which there is

homozygous *NF1* inactivation (3–6). Although loss of the second (wild-type functional) *NF1* allele presumably occurs randomly in tumor progenitors, the natural history of NF1-associated gliomas indicates that a non-random process influences where and when tumors grow. Gliomas in NF1 most frequently occur between the retina and the optic chiasm in a pattern referred to as “optic pathway” glioma (OPG). Remarkably, OPGs typically grow in young children and rarely progress after 10 years of age, regardless of treatment. These observations suggest that the growth of OPG in NF1 is developmentally regulated, and that regulatory signals from the surrounding brain microenvironment dictate when tumors are most likely to form and grow.

The molecular basis for this unique pattern of tumor growth in patients with NF1 has not been identified, but may be readily studied in two recently described genetically engineered models of NF1-associated OPG. Similar to human disease, mouse models of OPG indicate that glioma formation in NF1 requires cooperation between *Nf1* loss and additional factor(s) derived from the surrounding *Nf1*+/- brain (7, 8). Complete loss of neurofibromin expression in GFAP-expressing cells (*Nf1*^{fllox/fllox}; *GFAP-Cre*) results in hyperproliferative astrocytes, but is insufficient for glioma formation (9). In contrast, targeted loss of neurofibromin in GFAP-expressing cells in the context of an *Nf1*+/- brain (*Nf1*^{fllox/mut}; *GFAP-Cre*; *Nf1*+/-^{GFAP}CKO), similar to what occurs in patients with NF1, results in glioma formation. Under these conditions, tumors form along the optic nerve in young mice in which tumor cell proliferation is maximal between 3 weeks and 2 months and greatly reduced after 4–5 months of age (7, 10).

Neurofibromin functions as a GTPase-activating protein for the RAS proto-oncogene (11–17). Loss of neurofibromin expression in astrocytes results in KRAS hyperactivation (8, 18–22). Furthermore, activation of KRAS in GFAP-positive cells results in OPG formation, but similar to OPG in *Nf1*+/-^{GFAP}CKO mice, only in the context of an *Nf1*+/- brain (*Nf1*+/-; KRAS^{GFAP}; ref. 8). These observations indicate that tumorigenesis in NF1 requires cooperativity between loss of neurofibromin and developmentally regulated, growth-promoting signal(s) that originate from the surrounding *Nf1*+/- optic pathway.

The chemokine CXCL12 and its receptor CXCR4 represent compelling candidate cofactors for NF1-associated OPG formation. CXCL12 and CXCR4 are important patterning agents during normal brain development (23). In addition, paracrine activation of CXCR4 is necessary for malignant neural and astrocytic tumor xenograft growth *in vivo* (24). Furthermore, CXCR4 is a Gα_i-coupled receptor whose activation results in the stimulation of RAS and inhibition of cyclic AMP (cAMP) production (25). Neurofibromin loss, which is associated with both increased RAS activation and decreased production of cAMP, would be predicted

Note: Supplementary data for this article are available at Cancer Research Online (<http://cancerres.aacrjournals.org/>).

Requests for reprints: Joshua B. Rubin, Department of Pediatrics, Washington University School of Medicine, Box 8208, 660 South Euclid Avenue, St. Louis, MO 63110. Phone: 314-286-2790; Fax: 314-286-2892; E-mail: rubin_j@kids.wustl.edu.

©2007 American Association for Cancer Research.
doi:10.1158/0008-5472.CAN-06-2220

to enhance these CXCR4 effects (26–28). In the present study, we examine the hypotheses that the CXCL12-CXCR4 pathway acts cooperatively with neurofibromin loss in astroglial cells to enhance their growth potential, and that normal developmental regulation of CXCL12 expression and cAMP levels predisposes children with NF1 to astrocytoma growth along the optic pathway.

Materials and Methods

Chemicals, Reagents, and Antibodies

All chemicals were obtained from Sigma unless otherwise indicated. All tissue culture reagents and media were obtained from Invitrogen unless otherwise indicated. Antibodies and suppliers were as follows: phospho-Erk1/2 (pErk1/2), Erk1/2, phospho-Akt (pAkt), and Akt were from Cell Signaling; CXCR4 monoclonal antibody was from R&D Systems; CXCR4 polyclonal antibody was from Leinco; CXCL12 was from Peprotech; neurofilament 160 (NF160) was from Sigma; CD68 was from DakoCytomation; phospho-GRK2 was from Abcam; GRK2 was from Epitomics; and immunoglobulin G (IgG) isotype controls were from Jackson ImmunoResearch. A novel phospho-CXCR4-specific antibody (pCXCR4) was prepared and purified in our laboratory as previously described (29).

Tissue Samples

Human tissue. Paraffin-embedded OPG specimens from patients with NF1 ($n = 3$) and brain autopsy specimens ($n = 3$ from children <1 year of age; $n = 2$ from an 11- and a 12-year-old) were retrieved from the archives of the Department of Pathology at the Washington University School of Medicine in accordance with an Institutional Review Board–approved protocol for the use of human pathology specimens.

Rhesus macaque tissue. Pre-pubescent Rhesus macaque tissue was obtained from the Tulane National Primate Research Center.

Mouse Tissue. *Nf1*^{+/−}^{GEAP}*CKO* and *Nf1*^{+/−}; *KRAS*^{GEAP} mice were genotyped and tumors harvested as previously described (7, 8). All animals were used in accordance with established Animal Studies Protocols at the Washington University School of Medicine.

Tissue Sections and Immunohistochemistry

Tissue preparation and staining of 5- μ m sections was done as previously described (29). For evaluation of CD68 expression, slides were heated with Target Retrieval Solution (DakoCytomation) according to the manufacturer's instructions. Primary antibody concentrations were as follows: CXCR4 in human tissue, mouse monoclonal antibody (1 μ g/mL) and in mouse tissue, rabbit polyclonal antibody (1:200), CXCL12 (1:66), NF160 (1:150), CD68 (1:100), and pCXCR4 (1:66). Control sections were incubated with isotype-matched IgG.

Culture and Treatment of Primary Astrocytes

Primary cultures of astrocytes were prepared from postnatal day 2 *Nf1*^{lox/lox} mice as previously described (28). Cultures were infected with adenovirus containing either Cre recombinase (*Nf1*^{−/−}) or LacZ (*Nf1*^{+/+}). Primary cultures of astrocytes were grown under standard adherent conditions in serum-free media (DMEM/F12) or Neurobasal (Life Technologies-BRL) in the presence or absence of 0.1 μ g/mL CXCL12 (Peprotech), 10 μ mol/L forskolin for 24 h, 100 μ mol/L dideoxyadenosine, or 10 μ mol/L PD98059 as indicated. PD98059 was resuspended in DMSO, and in experiments involving PD98059, all cells were treated with equal concentrations of DMSO. Cell number was determined after 24 h by trypan blue exclusion. The growth effects of CXCL12 were derived as follows: [(cell number in the presence of CXCL12) − (cell number in the absence of CXCL12)] / [cell number in the absence of CXCL12] \times 100.

Primary Microglia Cultures

Primary murine microglia were isolated from mixed glial cultures derived from postnatal day 1 to 2 pups as previously described (30). Briefly, 15- to 20-day mixed glial cultures in six-well plates were trypsinized with 0.05% trypsin-EDTA, and an intact layer of astrocytes was detached and removed. Microglia attached to the wells were recovered by trypsinization with 0.25%

trypsin and vigorous pipetting. Isolated primary microglia were grown in mixed glial conditioned medium. Culture supernatants were collected after 72 h.

Western Blot Analysis

Whole-cell extracts were obtained by lysing cells with lysis buffer [20 mmol/L Tris (pH, 7.4), 137 mmol/L NaCl, 10% glycerol, and 1% Triton X-100] supplemented with phosphatase inhibitor cocktail set II (Calbiochem), phenylmethylsulfonyl fluoride (1 mmol/L), leupeptin (0.005 mg/mL), and aprotinin (0.005 mg/mL). The proteins were resolved with 10% Bis-Tris gels (Invitrogen) and transferred onto Hybond ECL nitrocellulose membrane (Amersham) according to standard protocols. Membranes were incubated with antibodies directed against pErk1/2 (1:1,000), Erk1/2 (1:500), pAkt (1:500), Akt (1:1,000), pGRK2 (1:250), GRK2 (1:500), pCXCR4 (1:500), CXCR4 (1:500), and actin (1:10,000) overnight at 4°C. This was followed by incubation with horseradish peroxidase-conjugated secondary antibody (1:15,000; Bio-Rad). Peroxide activity was detected using the enhanced chemiluminescence Supersignal West Dura system (Pierce). Quantitation of Western blots was done by densitometry using ImageJ software from the NIH. Differences in pCXCR4/CXCR4 ratios were calculated as the changes induced by CXCL12 and other treatments over time compared with baseline.

cAMP Measurements

The cAMP content of brain tissue and tissue culture cells was measured by ELISA (Cayman Chemical Company or Assay Designs) according to the manufacturer's directions as described (31).

CXCL12 Measurements

The CXCL12 content of microglial culture supernatants was measured by Quantikine SDF-1 α Immunoassay (R&D Systems) according to the manufacturer's directions.

Cell Cycle Analysis

Ethanol-fixed cells were washed in PBS and resuspended in PI staining solution containing 0.1% Triton X-100, 0.2 mg/mL RNase A, and 20 μ g/mL propidium iodide in PBS. Cells were incubated for 15 min at 37°C in the dark. Flow cytometry was done on a FACSCalibur system (Becton Dickinson). Data were analyzed using CellQuest software (Becton Dickinson). Aggregates and debris were excluded from the analysis.

Quantitative PCR

Mouse cortex, cerebellum, brainstem, and optic pathway (retina, optic nerves, optic chiasm, and supra-chiasmatic hypothalamus) were collected from *Nf1*^{+/+} and *Nf1*^{+/−} mice, and RNA was isolated from each region with TRIzol (Invitrogen) according to the manufacturer's instructions. Copy DNA was synthesized as described (24). CXCL12 and glyceraldehyde-3-phosphate dehydrogenase (GAPDH) transcripts were amplified from 125 ng of cDNA from each brain region using the SYBR GREEN PCR Master Mix (Applied Biosystems) according to the manufacturer's instructions. Primers for CXCL12 (forward primer, AAACCAGTCAGCCTGAGCTACC; reverse primer, GGCTCTGGCGATGTGGC) and GAPDH (forward primer, GGCAAAATCAACGGCACAGT; reverse primer, AGATGGTGATGGGCTTCCC) were obtained from Integrated DNA Technologies, Inc. and used at 35 μ mol/L and 50 μ mol/L, respectively. Samples were run in triplicate with a corresponding GAPDH control for each sample. PCR and data collection were done using the ABI 7500 machine and 7500 System SDS Software from Applied Biosystems. Relative transcript copy number for each CXCL12 and corresponding GAPDH sample was calculated in the following manner: $10^{(Ct - 40)/(-3.32)}$. The average of all replicates per sample was obtained, and the average CXCL12 copy number was divided by the average GAPDH copy number.

Terminal Nucleotidyl Transferase-Mediated Nick End Labeling Staining

Terminal nucleotidyl transferase-mediated nick end labeling (TUNEL) staining of fixed cells was done by standard procedures according to the manufacturer's directions (Roche Applied Science). TUNEL-positive cells were detected under direct fluorescence microscopy. TUNEL positivity was measured by the percent of total nuclei that were TUNEL positive.

Results

CXCR4 is present in a ligand-induced phosphorylated form in NF1-associated OPG. We analyzed OPG specimens from three patients with NF1 and identified three cellular sources of CXCL12. Similar to observations in sporadic low- and high-grade astrocytomas as well as medulloblastomas (24, 29, 31), CXCL12 was abundantly expressed in the endothelium of tumor-associated blood vessels (Fig. 1A-e). In addition, evaluations of serial sections from the same tumors revealed that CXCL12 was present in NF160-positive neuronal processes, representing entrapped axons, a common feature in OPG (Fig. 1B). CXCL12 was also detected in cells that were identified as parenchymal microglia by their expression of CD68 (Fig. 1C). Consistent with previous studies, CXCR4 was present in a ligand-induced phosphorylated form in cells with the typical elongated morphology of astrocytoma cells (Fig. 1D; ref. 29). These results show that the proximity of these multiple sources of CXCL12 to tumor cell CXCR4 comprises a functional paracrine relationship for CXCR4 activation. Intratumoral CXCL12 was also evident in OPG specimens derived from two mouse models of OPG, *Nf1*^{+/-}^{GEAP}*CKO* and *Nf1*^{+/-}; *KRAS*^{GEAP} mice (Supplementary Fig. S1A and B).

Developmental regulation of CXCL12 expression in the brain correlates with the temporal pattern of OPG growth. Based on the expression of CXCL12 and CXCR4 in NF1-associated OPG, we hypothesized that CXCL12 would modulate OPG growth in a manner analogous to its role in promoting malignant brain tumor growth. To determine whether developmental regulation of CXCL12 expression temporally correlated with the period of NF1-associated OPG growth, CXCL12 expression was examined in the brains of human infants and adolescents. In children <1 year of age, CXCL12 expression was localized in the vascular endothelium and ependymal cells throughout the brain, scattered neurons in the neocortex and Purkinje cells, and the pia mater overlying the external granule cell layer of the cerebellum (Supplementary Fig. S2A). CXCL12 expression was also evident in axons of the optic nerve and in the supra-chiasmatic portion of the hypothalamus (Fig. 2A). Significant optic nerve and hypothalamic CXCL12 expression was similarly observed in the brains of 3-week-old mice (Fig. 2B) and in the brain of a pre-pubescent Rhesus macaque (Supplementary Fig. S2B). Localization of CXCL12 to these brain regions is consistent with previous studies (reviewed in ref. 32).

Neuronal CXCL12 expression was significantly reduced in most brain areas in both the 11- to 12-year-old human brains (Fig. 2A) and the 3-month-old mouse brains (Fig. 2B) compared with their younger counterparts. The one exception was the cortex, where CXCL12 protein expression seemed comparable at all ages examined (Supplementary Fig. S2A). Developmental regulation of CXCL12 expression was also evident by quantitative RT-PCR analysis of mRNA derived from several regions of the mouse brain (Supplementary Fig. S2C). There were significantly decreased levels of CXCL12 mRNA in the brainstem and cortex and a trend toward decreased levels in the optic nerve and cerebellum of 19-week-old compared with 3-week-old mice.

In the cortex, we observed an apparent discordance between CXCL12 protein and mRNA levels. Immunostaining for CXCL12 seemed unchanged, whereas mRNA abundance decreased with age. We suspect that the lack of correlation reflects several factors including the nonquantitative nature of immunohistochemistry compared with RT-PCR and the potential for post-transcriptional regulation of CXCL12 expression (33).

Because OPG formation in NF1 seems to only occur in the context of an *Nf1* heterozygous tumor microenvironment (7), we next sought to determine whether mono-allelic loss of *Nf1* affects CXCL12 expression. We found no significant differences in the pattern or quantity of CXCL12 protein or mRNA expression between wild-type and *Nf1*^{+/-} mice (data not shown). However, none of the brains examined in these studies were derived from mice with OPG. Because there was increased CXCL12 expression within the mouse OPGs (see Supplementary Fig. S1A and B), we postulated that heterozygous loss of neurofibromin might alter the capacity of inflammatory cells to produce CXCL12. Human OPG analysis identified significant microglial infiltration (see Fig. 1). Therefore, we examined microglial expression of CXCL12 and found that primary cultures of *Nf1*^{+/-} microglia produce more than 3-fold greater amounts of CXCL12 compared with *Nf1*^{+/+} microglia (Fig. 2C). These data are consistent with mono-allelic *Nf1* loss, resulting in a greater potential for CXCL12 expression in the brain and, thus, a greater potential for CXCL12-dependent brain tumor growth.

Neurofibromin loss confers a CXCL12-mediated growth advantage in astrocytes. To determine the biological significance of CXCR4 activation to NF1-associated glioma biology, we evaluated neurofibromin regulation of CXCL12 growth effects. Although the true cell of origin of astrocytomas remains unknown, CXCR4 is known to be expressed early in the astrocyte lineage (34, 35) and is found in astrocytes, including those within the optic nerve (data not shown). Therefore, we used primary cultures of neocortical astrocytes as a model for astrocytoma precursor cells. Astrocytes were derived from postnatal day 2 *Nf1*^{lox/lox} mice and rendered *Nf1*^{+/+} or *Nf1*^{-/-} by infection with adenovirus encoding LacZ or Cre recombinase, respectively. In all experiments, infection with Ad5-Cre resulted in >95% reduction in neurofibromin expression as determined by Western blot (ref. 8; data not shown). Although *Nf1*^{+/+} and *Nf1*^{-/-} astrocytes express comparable levels of CXCR4 (Fig. 3A), markedly different growth responses to CXCL12 were observed. As previously reported, *Nf1*^{-/-} astrocytes grew

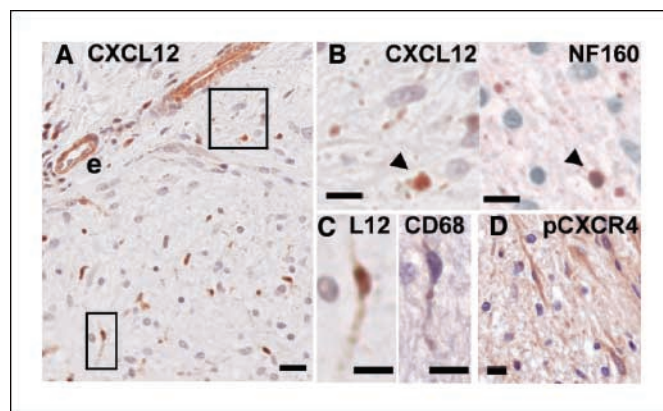
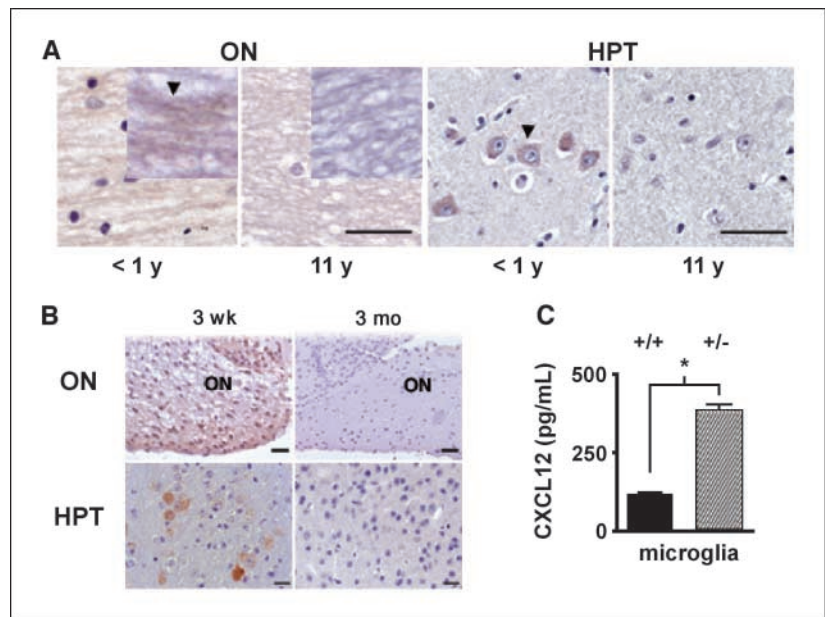


Figure 1. NF1-associated OPGs exhibit paracrine activation of CXCR4. A, representative NF1 OPG with typical histology was stained for CXCL12. Brown, positive staining. Vascular endothelium (e), cellular processes (top inset), and cells with typical morphology of microglia (bottom inset) all express CXCL12. Control IgG sections were negative (data not shown). B, top inset from (A) at higher magnification demonstrating CXCL12 staining of cellular process (arrowhead) that, in serial sections, is shown to also express neurofilament 160 (NF160). C, bottom inset from (A) at higher magnification (L12) and a cell of similar morphology stained for CD68. D, cells with typical morphology of astrocytoma cells express CXCR4 in a phosphorylated form (pCXCR4). Bars, 20 μ m for (A) and 10 μ m for (B-D).

Figure 2. CXCL12 expression in human and mouse brains is developmentally regulated. *A*, sections from autopsy brains of children <1 y of age and 11 y of age derived from optic nerve (ON) and hypothalamus (HPT) as indicated. *B*, sections of optic nerve and hypothalamus from 3-wk and 3-month-old mice as indicated. Brown, staining in all cases. Bars, 100 μ m for (A) and 20 μ m for (B). *C*, CXCL12 concentration in primary microglial culture supernatants was measured by ELISA. Columns, means of two separate experiments; bars, SD. *, $P < 0.05$ as determined by two-tailed *t* test.



more rapidly than *Nf1*^{+/+} astrocytes at baseline (data not shown). In addition, *Nf1*^{-/-} astrocytes responded to CXCL12 treatment (0.1 μ g/mL) with an increase in cell number of $14 \pm 2\%$, whereas *Nf1*^{+/+} astrocytes, under identical conditions, consistently showed a $10 \pm 5\%$ decrease compared with untreated controls (Fig. 3B).

The basis for the *in vitro* growth effects of CXCL12 was further evaluated by cell cycle analysis of asynchronously growing cultures of *Nf1*^{+/+} and *Nf1*^{-/-} astrocytes in the presence and absence of CXCL12. In agreement with the cell number measurements, 15% more *Nf1*^{-/-} astrocytes were in the S + G₂-M fraction of the cell cycle compared with *Nf1*^{+/+} astrocytes at baseline ($P < 0.005$, data not shown). CXCL12 treatment produced small changes in the fraction of proliferating (S + G₂-M) *Nf1*^{+/+} and *Nf1*^{-/-} astrocytes (data not shown). Consistent with previous studies of medulloblastoma and glioblastoma (24), the most significant effect of CXCL12 was on the fraction of cells undergoing apoptosis. This was determined by calculating the number of cells in the sub-G₀ fraction. Whereas *Nf1*^{+/+} astrocytes exhibited a $38 \pm 8\%$ increase in apoptotic cells, *Nf1*^{-/-} astrocytes showed a $27 \pm 12\%$ decrease in cells in the sub-G₀ fraction (Fig. 3C). The effect of CXCL12 on astrocyte apoptosis was confirmed by TUNEL analysis of parallel cultures (Fig. 3D).

CXCR4-mediated survival requires intracellular events in addition to the activation of MEK and phosphoinositide-3-kinase. Astrocyte growth has been linked to the activation of Erk1/2 (36) and phosphoinositide-3-kinase (PI3-kinase; ref. 37), and *Nf1*-deficient astrocytes exhibit high levels of RAS pathway activation (8). Consistent with these observations, treatment with the mitogen-activated protein/extracellular signal-regulated kinase (MEK) kinase inhibitor PD98059 or the PI3-kinase inhibitor wortmannin prevented the growth of *Nf1*^{+/+} and *Nf1*^{-/-} astrocytes (data not shown). To determine whether differences in the activation of MEK or PI3-kinase might underlie the differences in CXCL12 effects on *Nf1*^{+/+} versus *Nf1*^{-/-} astrocytes, we examined the activation (phosphorylation) of their downstream mediators, Erk1/2 and Akt. Although CXCL12 increased the phosphorylation of Erk1/2 and Akt in both *Nf1*^{+/+} and *Nf1*^{-/-} astrocytes, it did so to a similar degree (Fig. 4A),

suggesting that additional intracellular events must account for the differences in growth responses of *Nf1*^{+/+} and *Nf1*^{-/-} astrocytes to CXCL12.

cAMP is a known inhibitor of astrocyte proliferation (38, 39), whose generation is regulated by neurofibromin (28). Moreover, we have shown that CXCL12-stimulated brain tumor growth is

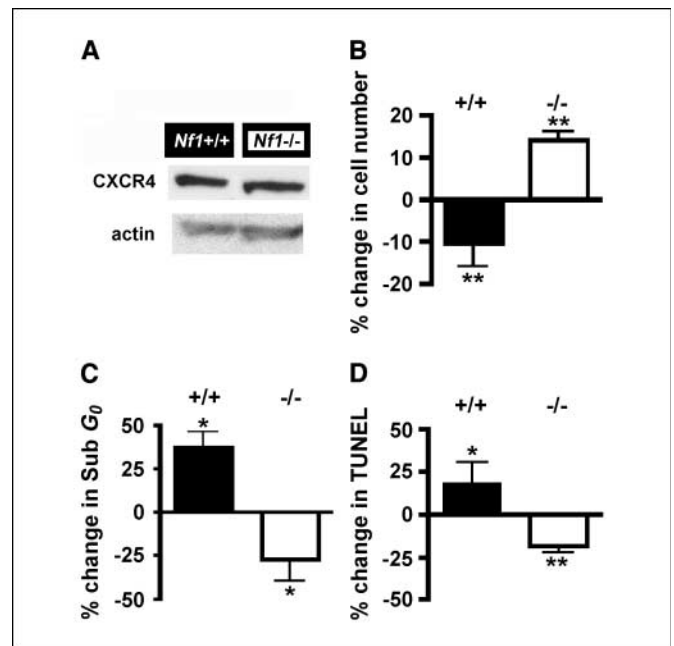


Figure 3. CXCL12 promotes the growth of *Nf1*^{-/-} but not *Nf1*^{+/+} astrocytes by decreasing apoptosis. *A*, *Nf1*^{+/+} and *Nf1*^{-/-} astrocytes in primary culture express comparable levels of CXCR4 as determined by Western blot analysis. β -Actin serves as loading control. *B*, CXCL12 growth effects on *Nf1*^{+/+} (filled columns, +/+) and *Nf1*^{-/-} (open columns, -/-) astrocytes. The contribution of apoptosis to changes in cell number was assessed by (C) flow cytometry (Sub-G₀) and (D) TUNEL analysis. *B*-*D*, columns, means of the three separate experiments done in duplicate (B and C) or quadruplicate (D); bars, SE. Significance for all experiments was determined by two-tailed *t* test; *, $P < 0.05$; **, $P < 0.005$.

dependent on the suppression of intracellular cAMP levels (31). Therefore, we evaluated whether differences in cAMP responses to CXCL12 were correlated with the differences in growth effects of CXCL12 on *Nf1*^{+/+} and *Nf1*^{-/-} astrocytes. Baseline levels of cAMP were comparable in *Nf1*^{+/+} (2.77 ± 0.34 pmol/mg protein) and *Nf1*^{-/-} (2.84 ± 0.07 pmol/mg protein) astrocytes and rapidly declined in response to CXCL12 (Fig. 4B). However, *Nf1*^{+/+} astrocytes exhibited oscillations in cAMP with a periodicity of ~10 to 15 min, which resulted in stereotypical responses consisting of three cAMP peaks during a 45-min experimental period. In contrast, the periodicity of cAMP oscillations was lengthened in *Nf1*^{-/-} astrocytes to ~20 to 30 min, producing only a single peak during the same experimental period. In addition to changes in the periodicity of cAMP oscillations, the integrated areas under each curve were different (*Nf1*^{+/+} astrocytes = 38.7; *Nf1*^{-/-} astrocytes = 28.7), indicating a 26% reduction in intracellular cAMP levels in *Nf1*^{-/-} astrocytes compared with *Nf1*^{+/+} astrocytes.

Growth response to CXCL12 is dependent on the suppression of cAMP. The above data suggested that CXCL12-induced *Nf1*^{-/-} astrocyte growth was dependent on decreased levels of intracellular cAMP. To test this hypothesis, we examined whether increasing intracellular cAMP levels would abrogate CXCL12-induced survival of *Nf1*-deficient astrocytes. We treated astrocytes with the adenylyl cyclase (AC) activator forskolin in the presence and absence of CXCL12. Baseline cAMP levels in *Nf1*^{+/+} and *Nf1*^{-/-} astrocytes were comparable (~3 pmol/mg of total protein). Forskolin elevated intracellular cAMP levels in both *Nf1*^{+/+} and *Nf1*^{-/-} astrocytes with peak values of 17.8 ± 0.4 and 19.4 ± 4.5 pmol/mg of protein, respectively, after 24 h of treatment. The effect of forskolin was not abrogated by cotreatment with CXCL12. Under these conditions, cAMP levels were 17.9 ± 2.5 and 10.4 ± 5.8 pmol/mg of total protein in *Nf1*^{+/+} and *Nf1*^{-/-} astrocytes, respectively. Moreover, we found that forskolin decreased *Nf1*^{+/+} astrocyte number and blocked CXCL12 growth-promoting effects in *Nf1*^{-/-} cells (Fig. 5A). The effect of forskolin on CXCL12-mediated *Nf1*^{-/-} astrocyte apoptosis was evidenced by changes in the percentage of *Nf1*^{-/-} astrocytes in the sub-G₀ fraction of the cell cycle (Fig. 5B).

To further evaluate the potential of decreased cAMP to stimulate *Nf1*^{-/-} astrocyte growth, we treated wild-type and *Nf1*^{-/-} astrocytes with the AC inhibitor dideoxyadenosine. Treatment with dideoxyadenosine lowered cAMP levels to 1.04 ± 0.9 and 0.68 ± 0.16 pmol/mg of total protein in *Nf1*^{+/+} and *Nf1*^{-/-} astrocytes, respectively. Similar to the effects of CXCL12,

dideoxyadenosine-induced cAMP suppression was associated with a decrease in *Nf1*^{+/+} and an increase in *Nf1*^{-/-} astrocyte cell number (Fig. 5C). As with CXCL12 treatment, changes in cell number were due to changes in apoptosis (data not shown). Thus, whereas astrocyte growth is dependent on MEK and PI3-kinase activity, CXCL12-induced *Nf1*^{-/-} astrocyte growth requires the suppression of intracellular cAMP levels.

Given the above findings, we evaluated whether brain region-specific differences in cAMP levels correlated with the pattern of glioma formation in NF1. The optic nerves, hypothalamus, cortex, cerebellum, and brainstem were isolated from 3-week-old *Nf1*^{+/+} and *Nf1*^{+/-} mice. Significant differences in tissue levels of cAMP (pmol/mg of protein) were evident between different brain regions as measured by ELISA (Fig. 5D). Cortex and hypothalamus showed the highest levels of cAMP (~2,500 pmol/mg protein). The cerebellum and brainstem exhibited intermediate levels of cAMP (~1,300 pmol/mg protein), and the optic nerves had the lowest levels of cAMP (~15 pmol/mg protein). Similar to the CXCL12 expression studies, there was no difference in cAMP levels between wild-type and *Nf1*^{+/-} brains. Thus, the preferential growth of NF1-associated gliomas along the optic pathway is consistent with the high level of CXCL12 expression and the low levels of cAMP found in this location.

Enhanced CXCL12-induced cAMP suppression is associated with decreased GRK2-mediated CXCR4 phosphorylation. The enhanced suppression of cAMP in *Nf1*^{-/-} astrocytes treated with CXCL12 suggested that CXCR4 desensitization had been diminished (40). Desensitization is an inhibitory feedback mechanism initiated when ligand-occupied G protein-coupled receptors (e.g., CXCR4) are phosphorylated by G protein receptor kinases (GRK). Phosphorylation promotes the binding of arrestins, thereby blocking further modulation of downstream targets such as AC (41). Failure to fully desensitize CXCR4 could therefore result in sustained inhibition of AC and suppression of cAMP. We found that CXCL12-induced CXCR4 phosphorylation was decreased in *Nf1*^{-/-} astrocytes compared with *Nf1*^{+/+} astrocytes (Fig. 6A). Although CXCL12 induced a 2.6 ± 0.06 -fold increase in pCXCR4 within 10 min in wild-type astrocytes, there was a 0.56 ± 0.14 -fold decrease in pCXCR4 in *Nf1*^{-/-} astrocytes at this time point. Thus, the first step in CXCR4 desensitization (phosphorylation) was diminished in *Nf1*^{-/-} astrocytes.

Decreased GRK-dependent phosphorylation could arise from changes in GRK expression or inhibition of GRK activity (42). GRK2 can phosphorylate CXCR4 (43) and is inhibited by Erk-mediated phosphorylation on Ser⁶⁷⁰ (44). Because Erk activity is increased as a

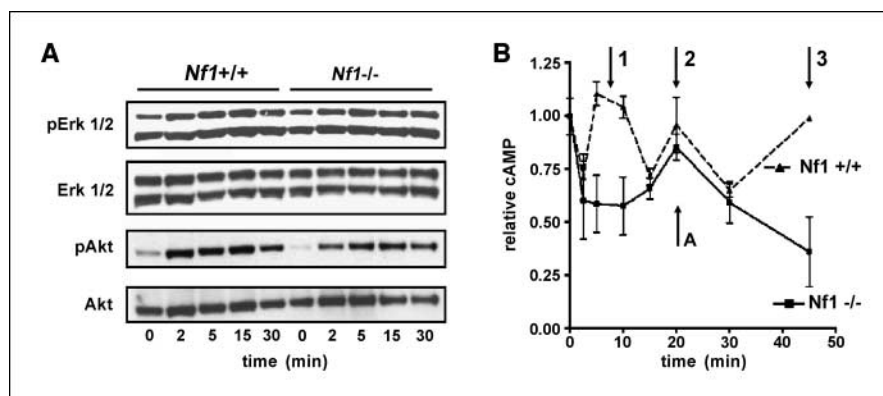
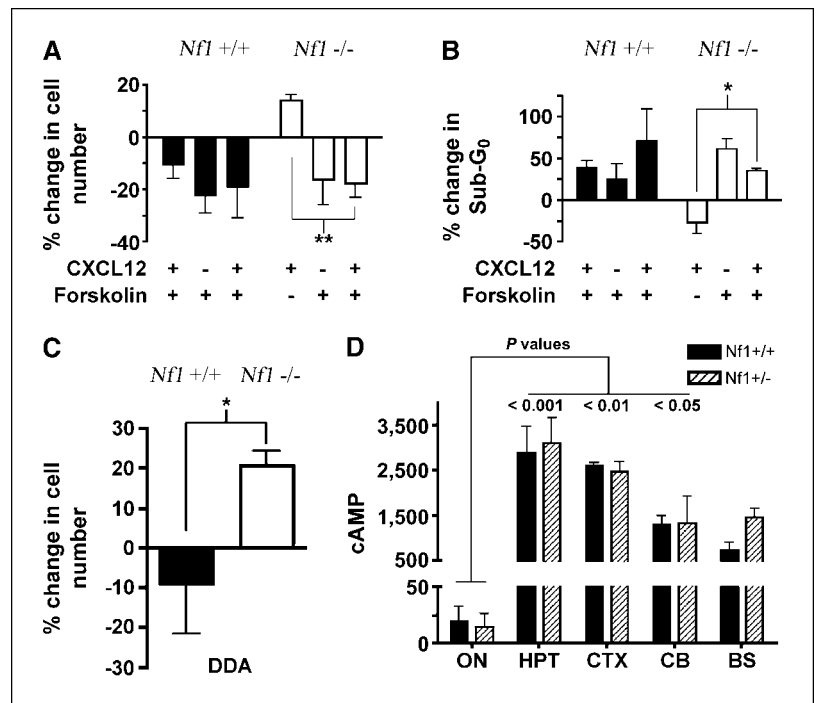


Figure 4. Loss of neurofibromin is associated with a change in cAMP responses to CXCL12. **A**, time-dependent changes in Erk 1/2 and Akt phosphorylation as a function of CXCL12 treatment ($0.1 \mu\text{g/mL}$) were determined by Western blot. Total Erk 1/2 and Akt serve as loading control. **B**, time-dependent changes in intracellular cAMP levels in *Nf1*^{+/+} (dashed line) and *Nf1*^{-/-} (solid line) astrocytes treated with CXCL12 ($0.1 \mu\text{g/mL}$) were measured by ELISA. Points, means of three separate experiments, each done in duplicate; bars, SE. Numbered arrows, peaks of cAMP response in *Nf1*^{+/+} astrocytes. Lettered arrow, single peak of cAMP response in *Nf1*^{-/-} astrocytes. The difference between the curves has a *P* value of <0.005 as established by two-way ANOVA.

Figure 5. Growth effects of CXCL12 are dependent on decreases in cAMP. *Nf1*^{+/+} (filled columns) and *Nf1*^{-/-} (open columns) astrocytes were cultured in the presence or absence of CXCL12 (0.1 μ g/mL) and forskolin (10 μ mol/L). **A**, cell number was determined by trypan blue exclusion. **B**, apoptotic fraction (sub-G₀ fraction) was measured by flow cytometry. **C**, effects of 24-h treatment with 100 μ mol/L dideoxyadenosine on *Nf1*^{+/+} (filled columns) and *Nf1*^{-/-} (open columns) astrocyte cell number. **D**, cAMP was isolated from optic nerve (ON), hypothalamus (HPT), cortex (CTX), cerebellum (CB), and brainstem (BS) of 3-week-old wild-type (*n* = 4) and *Nf1*^{+/-} (*n* = 4) mice as indicated and measured by ELISA. **Columns**, means; **bars**, SE. **P** values were determined with Bonferroni's multiple comparison test.



result of neurofibromin loss, we evaluated pGRK2 levels in *Nf1*^{-/-} and wild-type astrocytes. Although there was little to no pGRK2 present in wild-type astrocytes, a small but measurable amount was detected in *Nf1*^{-/-} astrocytes (Fig. 6B).

To determine whether increased Erk activity and GRK2 phosphorylation was related to the enhanced CXCL12-induced cAMP suppression in *Nf1*^{-/-} astrocytes, we treated wild-type and *Nf1*^{-/-} astrocytes with CXCL12 in the absence and presence of the MEK inhibitor PD98059 for up to 45 min. If increased Erk activation and GRK2 phosphorylation decreased CXCR4 desensitization (phosphorylation), then inhibition of MEK, the upstream activator of Erk, should restore normal CXCR4 desensitization (phosphorylation) and cAMP responses in *Nf1*^{-/-} astrocytes. Treatment with PD98059 inhibited Erk1/2 phosphorylation in both wild-type and *Nf1*^{-/-} astrocytes at all time points (Fig. 6C). Compared with no treatment, CXCL12 induced a 2.85 ± 0.17 -fold increase in peak CXCR4 phosphorylation in *Nf1*^{+/+} astrocytes. This peak was sustained between 2 and 10 min and was unaffected by PD98059. In contrast, whereas CXCL12 alone had no effect on pCXCR4 in *Nf1*^{-/-} astrocytes, cotreatment of *Nf1*^{-/-} astrocytes with CXCL12 and PD98059 resulted in a decrease in GRK2 phosphorylation and a 2.02 ± 0.37 -fold increase in peak (between 2 and 10 min) pCXCR4 levels. Thus, inhibition of Erk-mediated GRK2 phosphorylation restored CXCL12-induced CXCR4 phosphorylation.

Inhibition of Erk-mediated GRK2 phosphorylation also restored CXCL12-induced oscillations in cAMP levels. Similar to *Nf1*^{+/+} astrocytes, PD98059-treated *Nf1*^{-/-} astrocytes exhibited oscillations in cAMP with a periodicity of 10 to 15 min, resulting in three peaks during the 45-min experimental period (Figs. 4B and 6D). Moreover, PD98059 treatment abrogated the differences between *Nf1*^{+/+} and *Nf1*^{-/-} astrocyte cAMP levels over time (area under the curve: CXCL12-treated *Nf1*^{-/-} astrocytes, 27.17; CXCL12-treated *Nf1*^{+/+} astrocytes, 30.54; CXCL12/PD98059-treated *Nf1*^{-/-}

astrocytes, 30.38). These findings are consistent with a model of growth regulation in NF1 in which neurofibromin loss results in abnormal growth responses to CXCL12 as a consequence of decreased CXCR4 desensitization and enhanced CXCL12-induced cAMP suppression.

Discussion

The natural history of NF1-associated OPG in humans and genetically engineered *Nf1* mouse models indicates that tumor formation and growth are dependent on factor(s) from the surrounding brain microenvironment whose actions are developmentally regulated (3, 7). The data presented in this report support a model of gliomagenesis in NF1 in which microenvironment-derived CXCL12 works in concert with astrocyte neurofibromin loss to promote glioma formation and growth.

The interaction between neurofibromin loss and CXCL12 occurs on both a molecular and cellular level. On the molecular level, neurofibromin loss facilitates deregulated CXCR4 signaling as evidenced by decreased CXCR4 phosphorylation and sustained suppression of intracellular cAMP levels in CXCL12-treated *Nf1*^{-/-} astrocytes. Both of these effects indicate that CXCR4 desensitization is attenuated by neurofibromin loss. Moreover, CXCR4 desensitization and signaling was restored to near wild-type levels by treatment with PD98059. Based on these data, we propose that the increased RAS/MEK pathway activation in *Nf1*^{-/-} astrocytes results in decreased CXCR4 desensitization, mediated at least partly through MEK-dependent inhibition of GRK2.

Because human OPG contain large amounts of phosphorylated CXCR4, the inhibition of CXCR4 phosphorylation in *Nf1*^{-/-} cells must only affect acute responses rather than the steady-state levels measured by tumor tissue analyses. These acute effects are reflected by changes in the time course of CXCL12-induced CXCR4 phosphorylation in *Nf1*^{-/-} astrocytes. Thus, the *in vitro* data show

that CXCR4 signaling is altered in tumor cells, whereas the tissue analysis denotes the high levels of CXCL12 receptor binding found in tumor tissue.

On a cellular level, the reduction in apoptosis that occurs in response to CXCL12 augments the growth advantage associated with neurofibromin loss. In previous studies, the hyperproliferative state that results from neurofibromin loss or mutational KRAS activation in glia was shown to be insufficient for OPG formation (45, 46). Among the additional events that must work in concert with increased proliferation for oncogenesis to occur is the inactivation of apoptotic mechanisms (47). In this regard, our data supports the hypothesis that the inhibition of CXCR4 desensitization transforms normal CXCL12 signals into a co-stimulus for tumorigenesis. However, as autocrine or mutational activation of the CXCR4 pathway does not seem to occur in these tumors, the tumors remain dependent on microenvironment-derived CXCL12 for continued growth. In this fashion, the age-dependent decline in CXCL12 expression results in the cessation of tumor growth in already formed OPG and limits the development of new OPG.

Because CXCL12 is present in other regions of the brain, it is not obvious from measurements of CXCL12 expression alone why NF1-associated tumors preferentially form along the optic pathway. The tumor growth effects of CXCL12 are largely mediated by suppression of cAMP (31). In our current study, measurements of brain region-specific cAMP revealed that the optic nerve had the lowest intracellular cAMP levels. The second lowest cAMP levels

were measured in the brainstem, which is the second most common site for NF1-associated glioma formation. Based on these findings, it is probable that levels of intracellular cAMP dictate where tumors can grow. However, it should be recognized that cAMP levels are not likely to only reflect the actions of CXCL12. The relationship between CXCL12 receptor binding and resultant cAMP levels is also determined by expression and activity of $G\alpha_i$ -inhibitable AC, phosphodiesterases, GRKs, and other factors that regulate cAMP. The contributions of these regulatory proteins to modulating brain region-specific cAMP levels remain to be elucidated.

Although the anatomic differences in cAMP levels in the brain correlated with the localization of glioma formation in NF1 and the age-dependent expression of CXCL12 correlated with the temporal pattern of NF1-associated glioma growth, we did not observe any differences in CXCL12 expression or cAMP levels between wild-type and *Nf1*^{+/-} brains. For this reason, we cannot postulate that differences in CXCL12 or cAMP between wild-type and *Nf1* heterozygous brains influences tumor initiation. We did, however, find a significant difference in the capacity of wild-type and *Nf1*^{+/-} microglia to make CXCL12. It is well known that human NF1-associated OPG contain large numbers of infiltrating microglia. In tumor specimens, we found that microglia express high levels of CXCL12. Moreover, *Nf1*^{+/-} microglia express 3-fold higher levels of CXCL12 than their wild-type counterparts, raising the possibility that stroma-derived reactive cells, such as microglia, further drive glioma growth. In this regard, *Nf1*^{+/-} microglia could promote

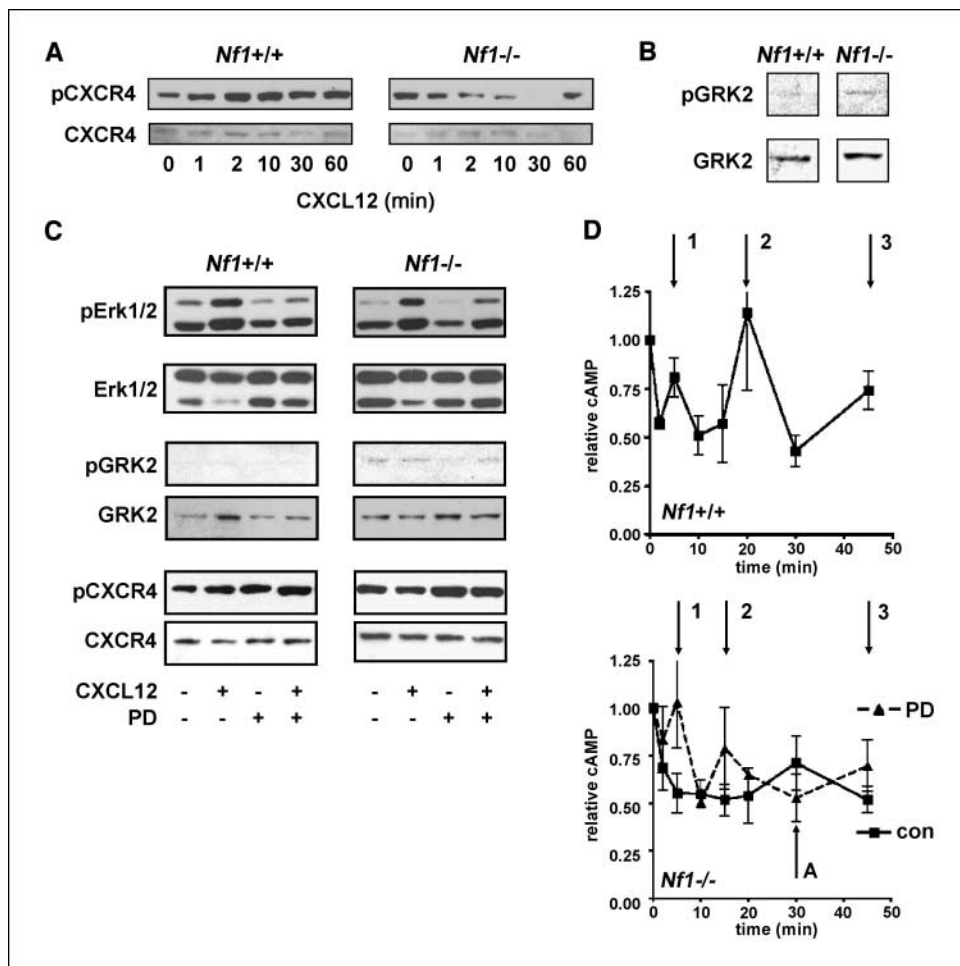


Figure 6. Neurofibromin loss inhibits CXCR4 phosphorylation via Erk-dependent phosphorylation of GRK2. **A**, CXCR4 phosphorylation (*pCXCR4*) was measured by Western blot analysis in primary cultures of *Nf1*^{+/+} and *Nf1*^{-/-} astrocytes treated with CXCL12 (0.1 μg/mL) for times indicated. Total CXCR4 served as control. **B**, level of phosphorylated GRK2 (*pGRK2*) in primary cultures of *Nf1*^{-/-} and *Nf1*^{+/+} astrocytes was measured by Western blot analysis. Total GRK2 serves as control. **C**, *Nf1*^{+/+} and *Nf1*^{-/-} astrocytes were cotreated with CXCL12 (0.1 μg/mL) and PD98059 (10 μM) for 0 to 45 min, and the phosphorylation of Erk1/2, GRK2, and CXCR4 was measured by Western blot analysis. Shown are representative blots of the 10-min time point. Total Erk1/2, GRK2, and CXCR4 serve as controls. The time course was repeated twice with similar results. **D**, the effect of PD98059 on cAMP responses was measured by ELISA. CXCL12-induced cAMP responses are compared in cultures of *Nf1*^{+/+} (top) to cultures of *Nf1*^{-/-} (bottom) astrocytes treated with CXCL12 alone (solid line, con) or cotreated with CXCL12 and PD98059 (dashed line, PD) for the times indicated. Baseline values for cAMP were comparable, *Nf1*^{+/+}, 3.46 ± 0.81 pmol/mg protein; *Nf1*^{-/-}, 2.5 ± 0.76 pmol/mg protein. Points, means of three separate experiments; bars, SE. Numbered arrows, peaks of cAMP response in *Nf1*^{+/+} and PD98059-treated *Nf1*^{-/-} astrocytes. Lettered arrow, single peak of cAMP response in *Nf1*^{-/-} astrocytes.

Nf1^{-/-} astrocyte growth and survival by providing CXCL12 or other mitogenic/survival factors (48). This is analogous to a model of dermal neurofibroma growth that depends on the infiltration of *Nf1*^{+/-} mast cells (49).

In summary, these studies provide the first mechanistic explanation for the unique pattern of NF1-associated OPG growth and suggest that OPG growth is dependent on ligand regulation of cAMP-dependent survival pathways. These findings raise the exciting possibility that similar mechanisms may underlie growth of other pediatric brain tumors with distinct patterns of formation, such as medulloblastoma, and suggest that these pathways may represent additional targets for therapeutic interventions.

Acknowledgments

Received 6/19/2006; revised 6/18/2007; accepted 7/9/2007.

Grant support: The U.S. Department of Defense (DAMD-17-01-0215 to D.H. Gutmann) and Schnuck Markets, Inc. (to D.H. Gutmann). B. Dasgupta and G.C. Dagainakatte were supported by nested postdoctoral fellowships from the U.S. Department of Defense. J.B. Rubin is a scholar of the Child Health Research Center of Excellence in Developmental Biology at Washington University School of Medicine and receives additional support from The Edward Mallinckrodt Jr. Foundation, The Children's Brain Tumor Foundation, and Hope Street Kids. The Tulane National Primate Research Center is supported by the NIH (RR00164).

The costs of publication of this article were defrayed in part by the payment of page charges. This article must therefore be hereby marked *advertisement* in accordance with 18 U.S.C. Section 1734 solely to indicate this fact.

The authors thank Dr. Ryan Miller for preparation of autopsy specimens and Drs. Louis Muglia, Robyn Klein, and Jonathan Gitlin for critical reading of the manuscript.

References

- Friedman J, Gutmann D, MacCollin M, Riccardi V. Neurofibromatosis: Phenotype, Natural History and Pathogenesis. 3rd ed. Johns Hopkins Press; 1999.
- Rubin JB, Gutmann DH. Neurofibromatosis type I—a model for nervous system tumour formation? *Nat Cancer Rev* 2005;5:557–64.
- Listernick R, Louis DN, Packer RJ, Gutmann DH. Optic pathway gliomas in children with neurofibromatosis 1: consensus statement from the NF1 Optic Pathway Glioma Task Force. *Ann Neurol* 1997;41:143–9.
- Gutmann DH, Donahoe J, Brown T, James CD, Perry A. Loss of neurofibromatosis 1 (NF1) gene expression in NF1-associated pilocytic astrocytomas. *Neuropathol Appl Neurobiol* 2000;26:361–7.
- Gutmann DH, James CD, Poyhonen M, et al. Molecular analysis of astrocytomas presenting after age 10 in individuals with NF1. *Neurology* 2003;61:1397–400.
- Kluwe L, Hagel C, Tatagiba M, et al. Loss of NF1 alleles distinguish sporadic from NF1-associated pilocytic astrocytomas. *J Neuropathol Exp Neurol* 2001;60:917–20.
- Bajenaru ML, Hernandez MR, Perry A, et al. Optic nerve glioma in mice requires astrocyte NF1 gene inactivation and Nf1 brain heterozygosity. *Cancer Res* 2003;63:8573–7.
- Dasgupta B, Li W, Perry A, Gutmann DH. Glioma formation in neurofibromatosis 1 reflects preferential activation of K-RAS in astrocytes. *Cancer Res* 2005;65:236–45.
- Bajenaru ML, Zhu Y, Hedrick NM, Donahoe J, Parada LE, Gutmann DH. Astrocyte-specific inactivation of the neurofibromatosis 1 gene (NF1) is insufficient for astrocytoma formation. *Mol Cell Biol* 2002;22:5100–13.
- Bajenaru ML, Garbow JR, Perry A, Hernandez MR, Gutmann DH. Natural history of neurofibromatosis 1-associated optic nerve glioma in mice. *Ann Neurol* 2005; 57:119–27.
- Ballester R, Marchuk D, Boguski M, et al. The NF1 locus encodes a protein functionally related to mammalian GAP and yeast IRA proteins. *Cell* 1990;63:851–9.
- Martin GA, Viskochil D, Bollag G, et al. The GAP-related domain of the neurofibromatosis type 1 gene product interacts with ras p21. *Cell* 1990;63:843–9.
- Xu GF, O'Connell P, Viskochil D, et al. The neurofibromatosis type 1 gene encodes a protein related to GAP. *Cell* 1990;62:599–608.
- Marchuk DA, Saulino AM, Tavakkol R, et al. cDNA cloning of the type 1 neurofibromatosis gene: complete sequence of the NF1 gene product. *Genomics* 1991;11: 931–40.
- Gutmann DH, Wood DL, Collins FS. Identification of the neurofibromatosis type 1 gene product. *Proc Natl Acad Sci U S A* 1991;88:9658–62.
- Andersen LB, Ballester R, Marchuk DA, et al. A conserved alternative splice in the von Recklinghausen neurofibromatosis (NF1) gene produces two neurofibromin isoforms, both of which have GTPase-activating protein activity. *Mol Cell Biol* 1993;13:487–95.
- Phillips RA, Hunter JL, Eccleston JF, Webb MR. The mechanism of Ras GTPase activation by neurofibromin. *Biochemistry* 2003;42:3956–65.
- DeClue JE, Papageorge AG, Fletcher JA, et al. Abnormal regulation of mammalian p21ras contributes to malignant tumor growth in von Recklinghausen (type 1) neurofibromatosis. *Cell* 1992;69:265–73.
- Burchill SA, Berry PA, Bradbury FM, Lewis JJ. Contrasting levels of p21ras activation and expression of neurofibromin in peripheral primitive neuroectodermal tumour and neuroblastoma cells, and their response to retinoic acid. *J Neurol Sci* 1998;157: 129–37.
- Bollag G, Clapp DW, Shih S, et al. Loss of NF1 results in activation of the Ras signaling pathway and leads to aberrant growth in haematopoietic cells. *Nat Genet* 1996;12:144–8.
- Guha A. Ras activation in astrocytomas and neurofibromas. *Can J Neurol Sci* 1998;25:267–81.
- Feldkamp MM, Angelov L, Guha A. Neurofibromatosis type 1 peripheral nerve tumors: aberrant activation of the Ras pathway. *Surg Neurol* 1999;51:211–8.
- Klein RS, Rubin JB, Gibson HD, et al. SDF-1 α induces chemotaxis and enhances Sonic hedgehog-induced proliferation of cerebellar granule cells. *Development* 2001;128:1971–81.
- Rubin JB, Kung AL, Klein RS, et al. A small-molecule antagonist of CXCR4 inhibits intracranial growth of primary brain tumors. *Proc Natl Acad Sci U S A* 2003; 100:13513–8.
- Peng H, Huang Y, Rose J, et al. Stromal cell-derived factor 1-mediated CXCR4 signaling in rat and human cortical neural progenitor cells. *J Neurosci Res* 2004;76: 35–50.
- The I, Hannigan GE, Cowley GS, et al. Rescue of a *Drosophila* NF1 mutant phenotype by protein kinase A. *Science* 1997;276:791–4.
- Guo HF, The I, Hannan F, Bernards A, Zhong Y. Requirement of *Drosophila* NF1 for activation of adenylyl cyclase by PACAP38-like neuropeptides. *Science* 1997;276:795–8.
- Dasgupta B, Dugan LL, Gutmann DH. The neurofibromatosis 1 gene product neurofibromin regulates pituitary adenylyl cyclase-activating polypeptide-mediated signaling in astrocytes. *J Neurosci* 2003;23: 8949–54.
- Woerner BM, Warrington NM, Kung AL, Perry A, Rubin JB. Widespread CXCR4 activation in astrocytomas revealed by phospho-CXCR4-specific antibodies. *Cancer Res* 2005;65:11392–9.
- Saura J, Tussell JM, Serratos J. High-yield isolation of murine microglia by mild trypsinization. *Glia* 2003;44: 183–9.
- Yang L, Jackson E, Woerner BM, Perry A, Pivnicka-Worms D, Rubin JB. Blocking CXCR4-mediated cyclic AMP suppression inhibits brain tumor growth *in vivo*. *Cancer Res* 2007;67:651–8.
- Klein RS, Rubin JB. Immune and nervous system CXCL12 and CXCR4: parallel roles in patterning and plasticity. *Trends Immunol* 2004;25:306–14.
- De La Luz Sierra M, Yang F, Narazaki M, et al. Differential processing of stromal-derived factor-1 α and stromal-derived factor-1 β explains functional diversity. *Blood* 2004;103:2452–9.
- Luo Y, Cai J, Liu Y, et al. Microarray analysis of selected genes in neural stem and progenitor cells. *J Neurochem* 2002;83:1481–97.
- Ehteshami M, Yuan X, Kabos P, et al. Glioma tropic neural stem cells consist of astrocytic precursors and their migratory capacity is mediated by CXCR4. *Neoplasia* 2004;6:287–93.
- Takuma K, Baba A, Matsuda T. Astrocyte apoptosis: implications for neuroprotection. *Prog Neurobiol* 2004; 72:111–27.
- Gomez Del Pulgar T, De Ceballos ML, Guzman M, Velasco G. Cannabinoids protect astrocytes from ceramide-induced apoptosis through the phosphatidylinositol 3-kinase/protein kinase B pathway. *J Biol Chem* 2002;277:36527–33.
- Pesic M, Drabek K, Esler C, Ruzdijic S, Pejanovic V, Pietrzakowski Z. Inhibition of cell growth and proliferation in human glioma cells and normal human astrocytes induced by 8-Cl-cAMP and tiiazofurin. *Nucleosides Nucleotides Nucleic Acids* 2000;19:963–75.
- Dugan LL, Kim JS, Zhang Y, et al. Differential effects of cAMP in neurons and astrocytes. Role of B-raf. *J Biol Chem* 1999;274:25842–8.
- Gainetdinov RR, Premont RT, Bohn LM, Lefkowitz RJ, Caron MG. Desensitization of G protein-coupled receptors and neuronal functions. *Annu Rev Neurosci* 2004;27:107–44.
- Ferguson SS, Barak LS, Zhang J, Caron MG. G-protein-coupled receptor regulation: role of G-protein-coupled receptor kinases and arrestins. *Can J Physiol Pharmacol* 1996;74:1095–110.
- Penn RB, Pronin AN, Benovic JL. Regulation of G protein-coupled receptor kinases. *Trends Cardiovasc Med* 2000;10:81–9.
- Orsini MJ, Parent JL, Mundell SJ, Marchese A, Benovic JL. Trafficking of the HIV coreceptor CXCR4: role of arrestins and identification of residues in the C-terminal tail that mediate receptor internalization. *J Biol Chem* 1999;274:31076–86.
- Pitcher JA, Tesmer JJ, Freeman JL, Capel WD, Stone WC, Lefkowitz RJ. Feedback inhibition of G protein-coupled receptor kinase 2 (GRK2) activity by extracellular signal-regulated kinases. *J Biol Chem* 1999;274: 34531–4.
- Bajenaru ML, Donahoe J, Corral T, et al. Neurofibromatosis 1 (NF1) heterozygosity results in a cell-autonomous growth advantage for astrocytes. *Glia* 2001; 33:314–23.
- Zhu Y, Harada T, Liu L, et al. Inactivation of NF1 in CNS causes increased glial progenitor proliferation and optic glioma formation. *Development* 2005;132:5577–88.
- Hanahan D, Weinberg RA. The hallmarks of cancer. *Cell* 2000;100:57–70.
- Dagainakatte GC, Gutmann DH. Neurofibromatosis-1 (NF1) heterozygous brain microglia elaborate paracrine factors that promote NF1-deficient astrocyte and glioma growth. *Hum Mol Genet* 2007;16:1098–112.
- Yang FC, Ingram DA, Chen S, et al. Neurofibromin-deficient Schwann cells secrete a potent migratory stimulus for NF1^{+/-} mast cells. *J Clin Invest* 2003;112: 1851–61.